Novel multivariate vector quantization for effective compression of hyperspectral imagery [☆]

Xiaohui Li [a], Jinchang Ren [b,*], Chunhui Zhao [a,*], Tong Qiao [b], Stephen Marshall [b]

[a] College of Information and Communication Engineering, Harbin Engineering University, Harbin, China
[b] Dept. of Electronic and Electrical Engineering, University of Strathclyde, Glasgow, UK

ARTICLE INFO

ABSTRACT

Although hyperspectral imagery (HSI) has been successfully deployed in a wide range of applications, it suffers from extremely large data volumes for storage and transmission. Consequently, coding and compression is needed for effective data reduction whilst maintaining the image integrity. In this paper, a multivariate vector quantization (MVQ) approach is proposed for the compression of HSI, where the pixel spectra is considered as a linear combination of two codewords from the codebook, and the indexed maps and their corresponding coefficients are separately coded and compressed. A strategy is proposed for effective codebook design, using the fuzzy C-mean (FCM) to determine the optimal number of clusters of data and selected codewords for the codebook. Comprehensive experiments on several real datasets are used for performance assessment, including quantitative evaluations to measure the degree of data reduction and the distortion of reconstructed images. Our results have indicated that the proposed MVQ approach outperforms conventional VQ and several typical algorithms for effective compression of HSI, where the image quality measured using mean squared error (MSE) has been significantly improved even under the same level of compressed bitrate.

1. Introduction

Hyperspectral imagery (HSI), through capturing hundreds of narrow and contiguous spectral bands from a wide range of the electromagnetic spectrum, has great capability in deriving comprehensive details about the spectral and spatial information of the ground material. As a result, it has been widely used in many remote sensing applications such as agriculture [1], mineralogy [2] and military surveillance [3].

In HSI, improved image quality is always desirable for better processing, which in turn results in a trend for an increase in spatial/spectral resolution, radiometric precision and a wider spectral range. Consequently, the data volume in the 3-D hypercube increases dramatically, resulting in challenges for data transmission, storage, and processing. To reduce the volume of data, effective coding and compression become a natural choice in this context.

Existing approaches for HSI compression can be divided into two main categories, i.e. lossless and lossy compression [4]. Lossless compression has been traditionally desired to preserve all the information contained in the image. However, the compression ratios which can be achieved with lossless techniques are limited. Lossless coding techniques include entropy coding and predictive modelling [5,6], where typical lossy compression approaches are transform based techniques [7,8] and vector quantization (VQ) [9,10]. In lossless compression such as predictive modelling, both intra-band spatial correlation and inter-band spectral correlation are used to determine a statistical model to estimate image values using partially observed data. The model and the estimation error are then encoded to represent the hypercube, where the performance relies on the correlation and statistical modelling [11,12].

Lossy compression yields higher compression ratio at the cost of introduced information loss. Despite the quality in the reconstructed image, these techniques are very popular, especially when the required compression could be achieved by lossy techniques. Moreover, the effect of the losses on specific applications in HSI have been assessed, such as target detection and data classification, showing that high compression ratio can be achieved with little impact in performance [7]. Several methods have been proposed for lossy compression of HSI, some of which are generalizations of existing 2D image or video algorithms, such as JPEG 2000 [13]. In [14], a Karhunen–Loeve transform was used to

compress hyperspectral cubes. Discrete wavelet transform and Tucker decomposition were applied in [8], while a pairwise orthogonal spectral transform was developed in [15]. Also, the H.264/AVC standard for video compression was applied to hyperspectral cubes [16]. Low-complexity paradigm which is based on a prediction stage, followed by quantization, rate-distortion optimization and entropy coding was proposed [17]. It leverages the simplicity and high-performance of prediction-based compression, requiring very few operations and memory, while advanced quantization and rate-distortion optimization ensure state-of-the-art compression performance.

In VQ-based lossy compression, the spectral signature of each pixel is used to determine an optimal codebook, which is then coded along with the indexed map of each spectral vector and transmitted for decoding. Although VQ-based approaches benefit from very high compression ratios for effective data reduction, they may suffer from significant distortion of image quality in coding and compression of HSI [9,18]. Since such degradation of image quality may lead to unrecoverable information loss in follow-on data analysis, the compression should be avoided as suggested in Ref. [19]. As a result, an ideal solution is to keep the quality and preserve essential information whilst the image is compressed.

To achieve this, a novel multivariate vector quantization (MVQ) approach is proposed. For the effective compression of HSI, the pixel spectra is considered as a linear combination of two codewords from the codebook rather than only one codeword as in the conventional VQ approach. To this end, for each spectral vector, two indexed maps and one or two coefficients are determined for coding. As a result, the information contained in the reconstructed imagery is better maintained than conventional VQ based approaches.

The remaining part of this paper is organised as follows. In Section 2, a strategy for codebook design based on FCM is presented. In Section 3, the proposed MVQ approach is presented, along with discussions of conventional VQ approach and techniques used in the MVQ approach. Experimental results and evaluations are presented in Section 4. Finally, some concluding remarks are drawn in Section 5.

2. The strategy for codebook design

In this section, a strategy of codebook design for coding and compression of HSI is presented, followed by the evaluation. Details regarding the associated technique, FCM, to be embedded in codebook design are also discussed.

2.1. Fuzzy C-mean algorithm

Developed by Dunn [34] and improved by Bezdek [20], fuzzy C-means (FCM) is a method of clustering which allows a data sample to belong to more than one cluster, yet with different degrees of membership. In general, FCM is based on minimization of the following objective function:

$$J_N = \sum_{i=1}^{N} \sum_{j=1}^{C} u_{ij}^m \mathbf{x}_i - \mathbf{c}_j^2 \tag{1}$$

where m is any real number greater than 1, u_{ij}^m is the degree of membership of pixel spectrum x_i in the cluster j, x_i is the ith of d-dimensional measured data, c_j is the d-dimension center of the cluster, and $||\ ||$ is any norm expressing the similarity between any measured data and the centre.

For fuzzy partitioning, an iterative optimization of the objective function is employed, where the degree of membership u_{ij} and the

cluster centres c_j are updated by

$$u_{ij} = \left\{ \sum_{k=1}^{C} \left(\frac{\mathbf{x}_i - \mathbf{c}_j}{\mathbf{x}_i - \mathbf{c}_k} \right)^{2/m-1} \right\}^{-1} \tag{2}$$

$$\mathbf{c}_j = \frac{\sum_{i=1}^{N} u_{ij}^m \times \mathbf{x}_i}{\sum_{i=1}^{N} u_{ij}^m} \tag{3}$$

This iteration stops when

$$max_{ij}\left\{ |u_{ij}^{(k+1)} - u_{ij}^{(k)}| \right\} < \delta \tag{4}$$

where δ is a pre-set termination criterion between 0 and 1; k is the iteration steps. This procedure converges to a local minimum or a saddle point of J_N.

2.2. Codebook design via blind clustering (CBC)

The best method of codebook design is to carry out an exhaustive search, which helps to determine an unstructured collection of codewords. As the full search is very time-consuming, a constrained search is usually employed to speed up this process to obtain a structured codebook. The approaches most commonly used for codebook design include the Linde, Buzo, Gray (LBG) algorithm [21], fuzzy vector quantization (FVQ) [22], Kekre's Fast Codebook Generation (KFCG) [23], and discrete cosine transform (DCT) based method.

In this paper, we present a codebook design strategy using a fuzzy C-mean (FCM) based blind clustering algorithm. According to the cost of FCM at different cluster numbers, the one with the minimum cost is chosen as the optimized cluster number. The cost in CBC is defined as follows:

$$C = N^\theta \times J_N \tag{5}$$

where N is the number of clusters, corresponding to N possible codewords; $\theta > 0$ is a constant, and J_N is an objective function of FCM when the data is clustered into N classes.

For a dataset, usually the sum of distortion J_N decreases with the rise of cluster numbers. If the codebook contains sufficient codewords, the distortion would approach zero. By combining the codebook size N into the defined cost function in (5), an adaptive solution for codebook design is achieved, where the codebook size and the final distortion is compromised.

2.3. Evaluation for codebook design strategy

To validate the efficacy of our proposed codebook design strategy, one simulated HSI dataset is used as an example and presented below. The simulated dataset has 30×30 pixel, including 6 classes represented in 6 vertical bars of a size 30×5 pixel, i.e. each class contains 150 pixel. Actually, the spectral data are extracted from the first HSI dataset, Salinas, as further described in Section 4, where in each class the 150 pixel are randomly selected within the corresponding class. The false colour images of the simulated hypercube are shown in Fig. 1 (left).

When CBC is applied for codebook design, 12 codewords are selected. Due to the spectral similarity of pixels from the same class, most codewords are actually selected from the corresponding class. This is illustrated in Fig. 1 (right), where pixels presented by the same colour belong to the same class.

3. Multivariate vector quantization approach

In this section, MVQ, the proposed approach for HSI compression, is presented. Relevant techniques along with descriptions of conventional VQ are introduced in detail below.
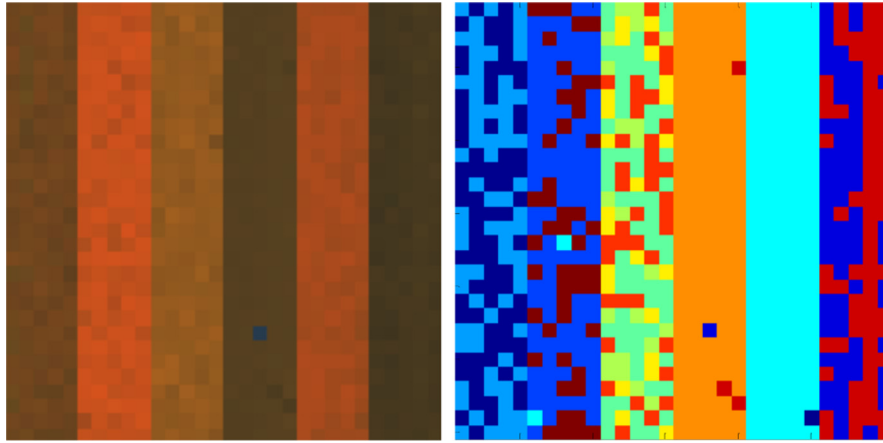
Fig. 1. Simulated image dataset in false colour (left, using the 50th, 100th and the 150th bands) and codewords of codebook determined using CBC (right). (For interpretation of the references to color in this figure legend, the reader is referred to the web version of this article.)

3.1. Conventional VQ approach (CVQ)

As a popular algorithm for image compression, CVQ is applied to vectors rather than scalars, and the latter is usually referred to as scalar quantization (SQ) [24]. SQ maps a large set of numbers to a smaller one, e.g. through rounding to the nearest code, although the quantization levels do not have to be evenly spaced. VQ rounds off or quantizes groups of numbers together instead of one at a time. These groups of numbers are called input vectors, and the quantization levels are called reproduction vectors, which are also the codewords from the codebook.

Note that VQ is a lossy compression technique. To specify a VQ encoder, one needs a set of reproduction vectors as the codebook, and a rule for mapping input vectors to the reproduction vectors. For an input vector, the VQ encoder maps it to one of the N possible reproduction vectors, where N is the number of codewords in the codebook. This reproduction vector is then selected as a codeword for the input vector. In addition to the codebook, only the index of the codeword needs to be coded in reconstructing the original vector for efficiency.

The mapping rule in VQ is defined to minimize an average distortion as follows. Let $d(\mathbf{Y}, \mathbf{X}_i) \geq 0$ measure the distortion or the cost of reproducing an input vector $\mathbf{Y}$ as a reproduction vector $\mathbf{X}_i$, the optimal $\mathbf{X}_i$ is simply determined as

$$d(\mathbf{Y}, \mathbf{X}_i) \leq d(\mathbf{Y}, \mathbf{X}_j), \quad \text{all} \quad j \tag{6}$$

In other words, the minimum distortion criterion in VQ encoder operates in the nearest neighbour fashion. In this case, the input vector can be presented as follows

$$\mathbf{Y} = \mathbf{X}_i + \boldsymbol{\varepsilon} \tag{7}$$

where $\boldsymbol{\varepsilon}$ is the residual usually neglected in lossy compression.

With the codebook and the indices of the codewords coded in the compressed image, decoding for image reconstruction is easily achieved in a simple lookup table. Upon receiving an index, the decoder puts out the stored codeword, the codeword in the codebook. The operation of the decoder is thus completely described once we have the specified codebook.

3.2. MVQ approach

Although CVQ has the advantages of simplicity and high data compression, in most cases it suffers from one series disadvantage, i.e. severe distortion of the image quality. This is because for each input vector of the original spectrum in CVQ, only one codeword from the given codebook is used for its approximated representation. As a result, the image distortion caused by the residual can be large, especially when the number of codewords is small.

To reduce this distortion, a multivariate vector quantization (MVQ) approach is proposed for the compression of HSI, where the spectral vector is considered as a linear combination of at least two codewords from the codebook. To this end, the residual and the image distortion is expected to be reduced for improved quality. However, the compression rate is degraded as two indexed maps and their corresponding coefficients need to be compressed and coded, rather than only one indexed map is needed in CVQ.

In the MVQ approach, the first model proposed is that the input vector is represented by a linear combination of two codewords from the codebook as follows

$$\mathbf{Y} = \alpha_1 \mathbf{X}_{i1} + \alpha_2 \mathbf{X}_{i2} + \epsilon_1 \tag{8}$$

where $\mathbf{X}_{i1}$ and $\mathbf{X}_{i2}$ refers to two codewords from the given codebook, while their corresponding coefficients are α_1 and α_2, and ϵ_1 is the residual which is neglected in lossy compression. In this model, there are two indices and two corresponding coefficients that need to be coded for compression. It is clear that the value of ϵ_1 in this new model is smaller than the value of ε in the CVQ approach. As a result, the distortion of image quality caused by the residual will be reduced.

For better data reduction, an improved MVQ model using only one coefficient for the two selected codewords is given below, which is a particular case of Eq. (8) where $\alpha_1 + \alpha_2 = 1$.

$$\mathbf{Y} = \beta \mathbf{X}_{i1} + (1 - \beta) \mathbf{X}_{i2} + \epsilon_2 \tag{9}$$

The residual ϵ_2 is also neglected in compression. In this model, two indices and one coefficient must be coded for each input vector. Again, the image distortion caused by the residual is smaller than that of CVQ resulting in better preservation of image information.

3.3. Multiple regression for parameter optimization

Based on the models defined in Eqs. (8) and (9), a multiple regression analysis is employed to solve the optimization problem in determining the associated parameters. The general purpose of the multiple regression is to learn more about the relationship between several independent variables. The general computational problem that must be solved in multiple regression analysis is to fit corresponding coefficients to the regression model. Thus, this general procedure is sometimes referred to as least squares

estimation. For the multiple regression

$$Y = f(X) + \theta \qquad (10)$$

Note that $f(X)$ is a known function, X is one of the probable codewords from the codebook, and θ is a random variable or vector, usually assumed to have expectation of 0. In most general terms, least squares estimation is aimed at minimizing the sum of squared deviations of the observed values for the dependent variable from those predicted by the model. Technically, the least squares estimator of the parameter θ is obtained by minimizing Q with respect to θ as

$$Q = d^2(Y, f(X)) \qquad (11)$$

where $d(\ )$ measures the distortion as defined in (6).

Regression aims to determine the optimal representation of the dependent variable Y, given the independent variables from the codewords X_i of the codebook ($i = 1, 2, …, n$). However, due to the complexity of the problem, it generates some residuals, i.e. the difference between the predicted values and the real observed data. As a result, the model with the minimum average residual is taken as optimal.

The residuals in multiple regression are often assumed to satisfy the normal distribution. For CVQ as given in Eq. (7), the function $f(X)$ is actually X_i. Since the corresponding coefficient is set as a constant 1, the only task is to select the appropriate codeword to minimise the residuals. To this end, the variable Y can be expressed in terms of a residual ε and an index i, denoting the selected codeword from the codebook X_i variable.

In the multivariate case such as the MVQ models defined in Eqs. (8) and (9), a linear equation is constructed by containing two variables X_{i1} and X_{i2}. Note that in these equations, the regression coefficients actually represent the contributions of each independent variable to the input vector of the dependent variable. Another way to express this property is to say that, for example, variable X_1 is correlated with the Y variable, after controlling for all other independent variables. This type of correlation is also referred to as a partial correlation.

3.4. Schemes for automatic codeword selection in MVQ

For correlation analysis, a common problem here is how to determine the most suitable one or more codeword measures X to represent a variable Y. In multiple regression analysis such as MVQ, this must be solved to determine the two codewords. Two schemes are used in our work, which are discussed in detail below.

Scheme A—two full searches: In this scheme, both the two codewords are determined using a full search of all possible combinations, which guarantees the least distortion in approximating the data for compression. However, it is the most time consuming as the multiple regression is computed N^2 times with the codebook size of N codewords. In each loop, the codeword has up to S possible options, where S refers to the number of pixels in the hypercube. To reduce the computational cost, another two schemes are given below, where one of the codewords is determined without a full search for efficiency.

Scheme B—one local search plus one full search: For a given variable Y, the first codeword is determined to be the most similar one from the codebook, based on the Euclidean distance of Y and the candidate codeword. Then, the second codeword is decided, through a full search. The computational cost of *Scheme B* contains $N-1$ loops of multiple regression and N times distance measurement of vectors, a dramatic reduction from N^2 loops of multiple regression as required in *Scheme A*.

In all regression techniques, there is a major conceptual limitation as one can only ascertain relationships rather than disclose underlying causal mechanism. In most real cases, causal

explanations are usually ignored provided that the regression achieves satisfactory results. To this end, the two schemes are presented for MVQ, where the results are compared in detail in Section 4.

4. Experimental results and analysis

For the MVQ approach proposed, four real HSI datasets are used in comprehensive experiments to validate its efficacy. Both subjective and objective evaluations are used for visual and quantitative assessment. Relevant results are presented below for comparisons.

4.1. Data preparation and experimental setup

The datasets used in this paper are collected by two well-known HSI spectrometers. The first is from the Airborne Visible/Infrared Imaging Spectrometer (AVIRIS), with spectral wavelengths ranging from 400 nm to 2500 nm in 224 contiguous bands. The second is the Reflective Optics System Imaging Spectrometer (ROSIS), which has 114 bands with a spectral range between 430 nm to 860 nm. Using the two sensors, four real HSI datasets, Salinas, Pavia, Indian Pines [25] and Moffett Field [26], are used in our experiments.

The 50th band images for these datasets are shown in Fig. 2. The Salinas dataset is an AVIRIS dataset collected over Salinas Valley, California (AVIRIS sensor) with a spatial size of 150×150 pixel, including 9 classes of different materials. The spatial resolution is 3.7 m. After discarding the water absorption bands, the remaining 204 bands of data are used. The Pavia dataset is collected from Pavia University, in Northern Italy (ROSIS sensor). It contains 103 bands with a spatial size of 150×150 pixel, including 9 classes of different materials. The spatial resolution of this HSI dataset is 1.3 m. The Indian Pines dataset is the public vegetation reflectance data from Indian Pines, northwest Indiana (AVIRIS sensor). Its spatial size is 145×145 pixel, with a spatial resolution of 20 m and 200 spectral bands (after removing bands covering the region of water absorption 104–108, 150–163 and 220). From 16 different land-cover classes available in the original ground truth data, 9 classes were selected to testify the effectiveness of methods in this paper. The Moffett Field dataset collected from California at the southern end of San Francisco Bay, USA, this dataset is widely used in hyperspectral community. Its spatial size is 512×512, with a spatial resolution of 20 m. This image comprises 224 bands recorded at different wavelengths in the range 380 nm to 2500 nm, with a nominal spectral separation of 10 nm between two adjacent bands.

In our experiments, each of the first three datasets is compressed using both CVQ and the proposed MVQ approach. Various results under two VQ models as defined in Eqs. (8) and (9) and various codeword selection schemes are also compared. In total there are up to 4 combinations of different conditions when the MVQ is applied, which are summarized in Table 1 for clarity. In addition, the CVQ approach is also extended as CVQ_E to allow a similar bitrate that MVQ achieved. The performance of these approaches is evaluated in detail as follows.

For performance assessment, three criteria are used for the first three datasets, which include compression bitrate (CBR), mean squared error (MSE) and the overall distortion (OD). As a commonly used metrics, CBR is used to measure the degree of data reduction. Let the original hypercube contain P bands sized of $M \times N$, where each pixel per band is represented in L bits, the uncompressed image size is $MNPL$ in bits. Denote N_{bit} as the total bits of the compressed hypercube, the compressed bit rate is
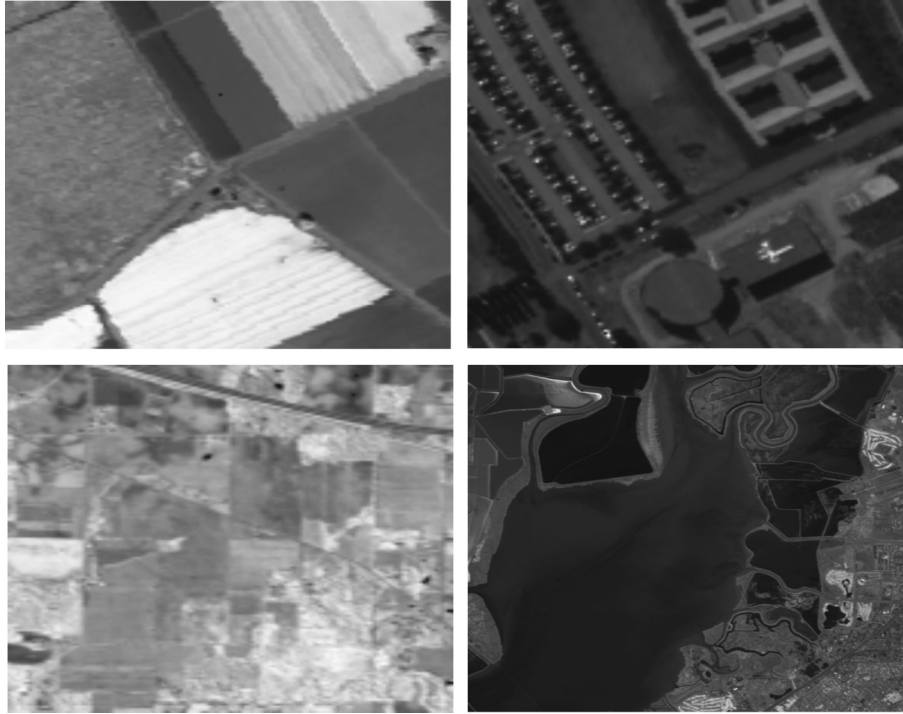
Fig. 2. The 50th band of the three HSI datasets: Salinas (top left), Pavia (top right) Indian Pines (bottom left) and Moffett Field (bottom right).

Table 1
Summary of different approaches used for benchmarking and comparisons.

Name	Compression approach	Multivariate VQ model	Codeword selection schemes
MVQ1a	Multivariate VQ (MVQ)	Eq. (8) with two parameters	A (two full searches)
MVQ1b			B (local+full search)
MVQ2a		Eq. (9) with one parameter	A (two full searches)
MVQ2b			B (local+full search)
CVQ	Conventional VQ		
CVQ_E	Extended CVQ to have similar bitrate as MVQ		

Table 2
CBR and MSE of different approaches.

Dataset	Salinas		Pavia		Indian Pines	
	CBR	MSE	CBR	MSE	CBR	MSE
CVQ	0.108	4.43	0.049	47.95	0.213	12.57
MVQ1a	0.194	0.64	0.138	7.28	0.306	7.68
MVQ1b	0.193	0.79	0.129	9.95	0.303	8.18
MVQ2a	0.169	1.51	0.112	16.3	0.274	8.74
MVQ2b	0.161	1.85	0.104	22.81	0.267	9.54
CVQ_E	0.17	3.29	0.131	28.59	0.293	12.36

defined as

$$\text{CBR} = \frac{N_{\text{bit}}}{LMNP} \tag{12}$$

where a lower CBR indicates that less bits are needed for compression hence the data is better compressed. However, the image may contain large distortion and resulting in low quality.

To measure the distortion of image quality, OD and MSE are used for visual and quantitative assessment, respectively. Let $\boldsymbol{X}$ and $\boldsymbol{X}'$ denote the original hypercube and the reconstructed hypercube, respectively. For OD, it measures pixel-based distortion over all the bands, which in practice provides a distortion image for visual inspection. For a given spatial location at (i, j), its OD measurement

is defined as

$$OD_{ij} = \sum_{k=1}^{P} |\boldsymbol{X}_{ijk} - \boldsymbol{X}'_{ijk}| \tag{13}$$

For MSE, it measures the average distortion over the whole hypercube and can be derived from OD below:

$$MSE = \frac{1}{MNP} \sum_{i=1}^{M} \sum_{j=1}^{N} \sum_{k=1}^{P} (\boldsymbol{X}_{ijk} - \boldsymbol{X}'_{ijk})^2 \tag{14}$$

When using the Cuprite dataset to compare the performance with other approaches, the signal-to-noise ratio (SNR) is also used to measure the quality of compression as defined below.

$$SNR = 10\log_{10} \frac{\text{Signal power}}{\text{MSE}} \tag{15}$$

where the Signal power for the hypercube $\boldsymbol{X}$ is defined as

$$\text{Signal power} = \frac{1}{M \times N \times P} \sum_{i=1}^{M} \sum_{j=1}^{N} \sum_{k=1}^{P} \boldsymbol{X}_{ijk}^2 \tag{16}$$

4.2. Results from the first three datasets

For MVQ approaches using CBC based codebook design, results from various conditions are summarized in Table 2 for performance evaluation. These include MVQ1a, MVQ1b, MVQ2a and MVQ2b as

well as CVQ and CVQ_E. The corresponding CBR and MSE values achieved are tabled for comparisons.

First, CVQ yields the least CBR for these three test datasets, i.e. the best data compression rate, at the cost of the maximum image distortion measured by MSE. In other words, CVQ fails to preserve the image quality for compression.

Second, all the four MVQ approaches produce much lower MSE, though the CBR measures are slightly higher. In addition, codeword selection *Scheme A* tends to generate a lower MSE than *Scheme B*, as the two codewords are globally selected to minimize the image distortion. However, the CBR from the two schemes are comparable, where *Scheme B* outperforms *Scheme A* in this context.

In addition, the VQ model with two parameters, i.e. MVQ1a and MVQ1b, generates smaller MSE but greater CBR in comparison to the results from MVQ2a and MVQ2b where the single parameter VQ model is used. Again, this is because the two-parameter model is able to achieve the best solution in reducing the MSE, yet the

additional parameter needed has inevitably decreased the CBR.

For the CVQ_E approach, it is adjusted from CVQ to have similar CBR as MVQ approaches. As can be seen, although the CBR measures are comparable or worse than those from MVQ, the corresponding MSE are much higher. This indicates that CVQ has fundamental limitations in maintaining a good image quality for compression, and this no doubt reflects the importance of the proposed MVQ approaches in this field.

In the following part, the image distortion is compared via visual inspection using the OD measurement. For better visualization, the outliers in the generated OD images are suppressed using a logarithmic mapping below.

$$OD'_{ij} = \log_2(1 + OD_{ij}) \tag{17}$$

For the Salinas dataset, the generated OD images are shown in Fig. 3 for comparisons. As can be seen, large distortion can be found again from CVQ and CVQ_E, whilst MVQ approaches yield
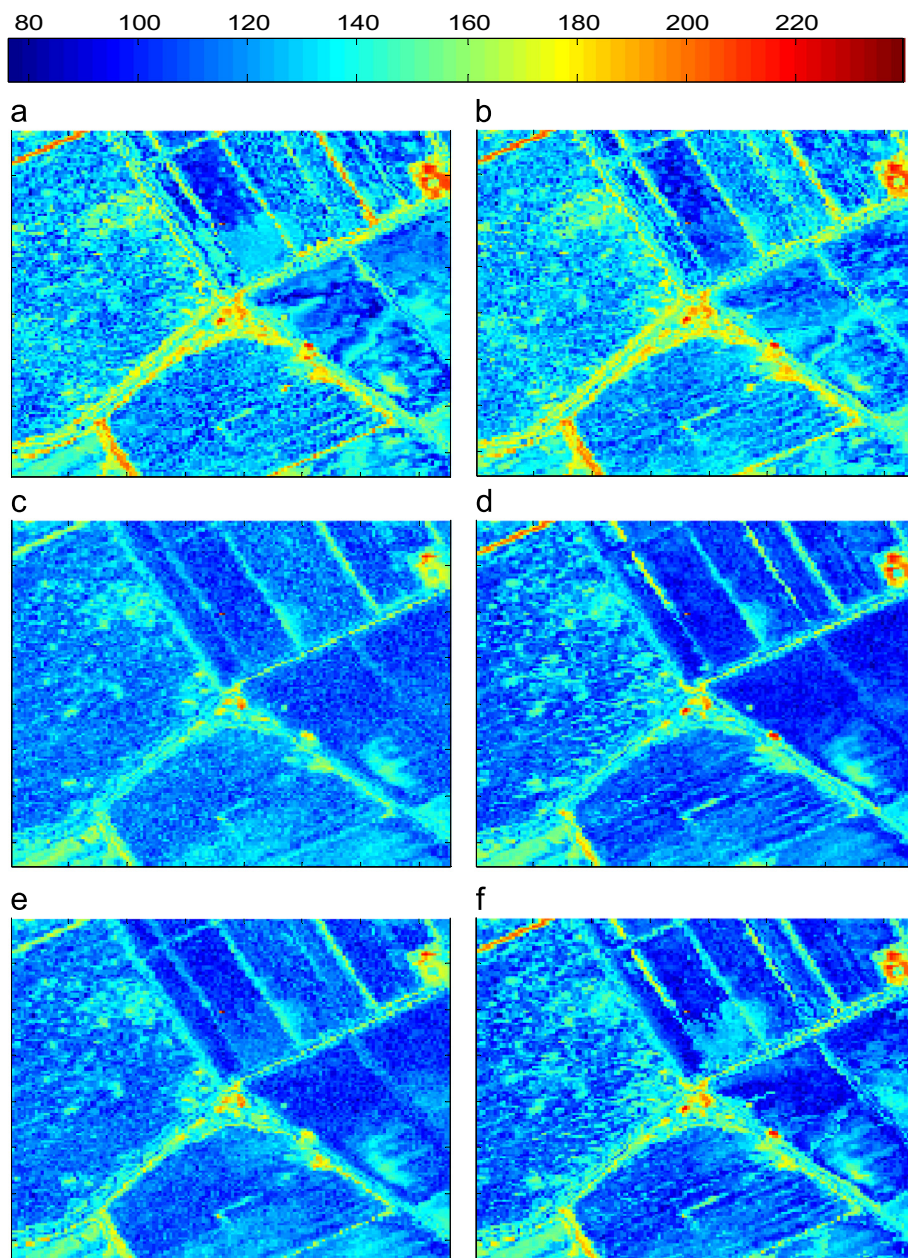

Fig. 3. Overall distortion of every pixel for the Salinas dataset: (a) CVQ, (b) CVQ_E, (c) MVQ1a, (d) MVQ2a, (e) MVQ1b, and (f) MVQ2b.

much less distortion. In most cases, distorted pixels are located near the edges of classes, i.e. high frequency components. Also we can see that distorted pixels from MVQ are usually contained in the results from CVQ/CVQ_E approaches. This has clearly shown
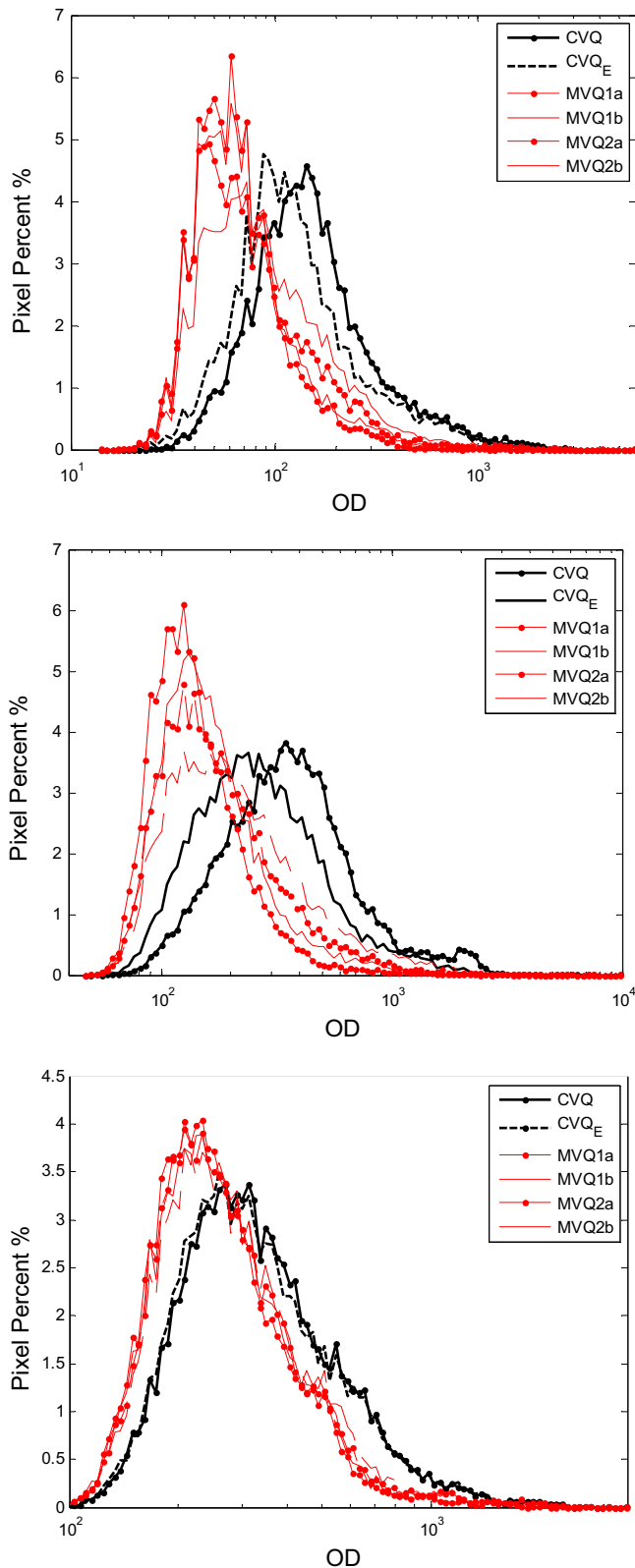
how the proposed MVQ approaches reduce the distortion for improved image quality.

For the four MVQ approaches, although the results from MVQ1a and MVQ1b have lower MSE than those from MVQ2a and MVQ2b as illustrated in Table 2, the visual effects are somewhat different. In fact, MVQ2a seems to yield less distortion for pixels within small homogeneous region, especially the right part of the image, though the distortion for the large block to the left and the un-homogeneous region is slightly higher. As those pixels tend to have large variations, this indicates that MVQ2a with the one parameter VQ model is more suitable in dealing with homogeneous images.

Since the OD images for the other two datasets are similar to those in Fig. 3, they are omitted in the paper. Instead, their histograms are used for comparisons. As shown in Fig. 4, results from CVQ approaches tend to have larger distortion and higher standard derivation (wide spread for inconsistency). On the other hand, MVQ approaches yield much reduced distortion and lower standard derivation. Although CVQ_E generates slightly improved results than CVQ, in principle they are quite comparable, especially for the Indiana Pines dataset. Results from the four MVQ approaches are also comparable to each other, though MVQ1a/MVQ1b seems to have fewer pixels with higher distortion in the right-side of the plotted curves.

From these histograms, we further derive the mean value of each histogram as the mid-value distortion (MVD) and the percentage of pixels over a fixed distortion threshold (PPD) for quantitative evaluations. The MVD and PPD measurements for the three datasets are compared in Table 3, where the fixed distortion thresholds are set as 100, 300 and 300, respectively.

Although it is difficult to compare the performance in Fig. 4, Table 3 has clearly shown the difference among these approaches. Disregarding the high MVD and PPD values from CVQ and CVQ_E, the four MVQ approaches can now be compared in detail. Although they are quite comparable, MVQ1a seems to produce slightly better results than other MVQ approaches.

Finally, running times of CVQ and the proposed MVQ on the three datasets are compared in Table 4 as an indicator of computational complexity. Although the absolute time consumed in these approaches also depends on the spatial dimension and the number of bands of the hypercube, for a given dataset the running time still provides a consistent measurement of complexity in this context. All the simulations are performed using Matlab R2012a on a Core™ 2 processor at 2.4 GHz with a Windows 8 system.

As can be seen, in general, MVQ, compared with CVQ, requires slightly more time for all the three datasets, whilst the reason behind is that MVQ needs to compress more data maps and their coefficients. In fact, the most time-consumption part in MVQ is to choose the best combination of codewords which is achieved by using multiple regression. Also, among these results of MVQ, *Scheme B* use less time than *Scheme A* as *Scheme B* only has one coefficient. For the same scheme, the two models require similar

Fig. 4. Comparing histograms of the OD images for the three datasets Salinas (top), Pavia (middle), and Indian Pines (bottom).

Table 3
MVD and PPD of different approaches.

Dataset	Salinas		Pavia		Indian Pines	
	MVD	PPD/%	MVD	PPD/%	MVD	PPD/%
CVQ	142.84	71.39	346.71	59.19	313.26	55.10
MVQ1a	60.71	15.86	131.15	6.07	241.76	32.77
MVQ1b	64.53	19.60	146.11	10.76	250.88	35.49
MVQ2a	64.53	26.02	154.22	16.19	250.88	35.83
MVQ2b	77.53	35.79	191.40	24.73	260.34	39.76
CVQ_E	111.86	57.18	250.74	38.21	313.26	53.14

Table 4
Running time in seconds of the three approaches over the three datasets.

Images and their pixels/bands		CVQ	MVQ1a	MVQ1b	MVQ2a	MVQ2b
Salinas	22,500/204	0.64	1.84	1.83	1.42	1.48
Pavia	22,500/103	0.47	1.76	1.77	1.41	1.41
Indian Pines	21,025/200	0.79	1.97	1.94	1.53	1.57

Table 5
Performance comparison using *SNR* with other approaches.

Approach (at 0.1 bpppb)	SNR
3D-SPIHT	12.92
3D-SPECH	12.60
JPEG 2000 multi component	10.79
2D-SPECH	14.61
LVQ-SPECH	15.38
CVQ	10.96
MVQ	17.83

running time. However, the additional time introduced seems a reasonable cost for the preserved image quality as illustrated in Tables 2 and 3.

4.3. Benchmarking with other approaches

In this section, our proposed MVQ methods are compared with non-MVQ approaches, where the widely used HSI dataset, Moffett Field, is employed for comparisons.

Three non-VQ and two VQ-based approaches are used for benchmarking, including 3D-SPIHT, 3D-SPECK algorithms [27], Multi Component feature of JPEG2000 [13], the original 2D-SPECK codec and CVQ. Table VI presents a comparison of the *SNR* results when processed by those approaches. Although the experimental conditions can be different when the results were generated as reported in [28], they can provide relatively consistent comparisons.

The results from these approaches and CVQ/MVQ2b approaches are given in Table 5 for comparisons of *SNR* with a fixed CBR, where the best MVQ approach, MVQ1a, is not used for fairer assessment. With a fixed CBR rate set at 0.1 bpppb, all approaches used for benchmarking have lower *SNR* yielded. In contrary, VQ based approaches generates significant less CBR for better data compression whilst the *SNR* has been maintained to an even high level, especially for the proposed MVQ approach. Based on Table VI, we see that the performance achieved by the MVQ algorithm is quite competitive, where it outperforms other non-MVQ approaches, when applied to scenes of the Moffet Field image.

5. Conclusions

In this paper, after applying a strategy for codebook design based on fuzzy C-mean (FCM) algorithm, a multivariate vector quantization (MVQ) approach is proposed for the compression of HSI, where the pixel spectra is considered as a linear combination of two codewords from the codebook, and the indexed maps and their corresponding coefficients are compressed and coded separately. With the strategy for codebook design under two codeword selection schemes, the performance of the proposed MVQ approach has been fully validated and assessed using three publically available hyperspectral datasets. MVQ approaches generate significantly reduced image distortion with a cost of slightly

increased CBR. Due to the fundamental limitation of CVQ, even its extended version fails to reach the performance as MVQ does.

Since MVQ approaches need to determine parametric models in optimize the VQ problem, it naturally has a high computation cost. However, the high computational cost is only for the offline coding stage, where the decoding stage has similar complexity to CVQ. For the two schemes used for codeword selection, *Scheme A* is more expensive than *Scheme B*. Accordingly, in general, *Scheme A* produces less MSE.

Although there is no single rule to choose the best MVQ approaches here, the two parameter VQ model, especially MVQ1a, outperforms the one parameter model in terms of less MSE hence better image quality. However, it usually has a larger CBR generated. For a given dataset, a good compromise between CBR and MSE in consideration of the variations in the images is always useful in determining the best MVQ approach in this context. In addition, how to derive a universal codebook for generic MVQ-based compression of hyperspectral images will be further investigated in the near future. Moreover, in combination of principal component analysis, singular spectral analysis, sparse representation and other relevant approaches [29–33], the proposed approach will be further improved.

References

[1] L. Tits, B. Sorners, P. Coppin, IEEE Trans. Geosci. Remote Sens. 50 (2012) 2273.
[2] R.J. Murphy, S.T. Monteiro, S. Schneider, IEEE Trans. Geosci. Remote Sens. 50 (2012) 3066.
[3] M.T. Eismann, A.D. Stocker, N.M. Naserbadi, Proc. IEEE 97 (2009) 1031.
[4] J. Wen, C. Ma, P. Shui, Opt. Commun. 284 (2011) 54.
[5] J. Mielikainen, B. Huang, IEEE Geosci. Remote Sens. Lett. 9 (2012) 1118.
[6] Y. Liang, J. Li, K. Guo, Opt. Express 20 (2012) 8199.
[7] B. Penna, T. Tillo, E. Magli, G. Olmo, IEEE Trans. Geosci. Remote Sens. 45 (2007) 1408.
[8] A. Karami, M. Yazdi, G. Mercier, IEEE J. Sel. Top. Appl. Earth Obs. Remote Sens. 5 (2012) 444.
[9] S.-E. Qian, IEEE Trans. Geosci. Remote Sens. 42 (2004) 1791.
[10] S.-E. Qian, M. Bergeron, I. Cunningham, L. Gagnon, A. Hollonger, IEEE Trans. Aerosp. Electron. Syst. 42 (2006) 851.
[11] C.-C. Lin, Y.-T. Hwang, J. Inf. Sci. Eng. 27 (2011) 419.
[12] H. Chen, Y. Zhang, J. Zhang, Y. Chen, IEEE Trans. Geosci. Remote Sens. 4 (2010) 3913.
[13] D.S. Taubman, M.W. Marcellin, JPEG2000 Image Compression Fundamentals, Standards and Practice, Springer US2002.
[14] Q. Du, J.E. Fowler, IEEE Geosci. Remote Sens. Lett. 4 (2007) 201.
[15] I. Blanes, J. Serra-Sagrista, IEEE Trans. Geosci. Remote Sens. 49 (2011) 961.
[16] L. Santos, S. Lopez, G.M. Callico, J.F. Lopez, R. Sarmiento, IEEE J. Sel. Top. Appl. Earth Obs. Remote Sens. 5 (2012) 451.
[17] A. Abrardo, M. Barni, E. Magli, IEEE Int. Conf. Acoust. Speech Signal Process. 2011 (2011) 797.
[18] S.-E. Qian, IEEE Trans. Image Process. 15 (2006) 2422.
[19] E. Christophe, D. Leger, C. Mailhes, IEEE Trans. Geosci. Remote Sens. 43 (2005) 2103.
[20] J.C. Bezdek, Pattern Recognition With Fuzzy Objective Function Algorithms, Kluwer Academic, Norwell, MA, USA, 1981.
[21] Y. Linde, A. Buzo, R.M. Gray, IEEE Trans. Commun. 28 (1980) 84.
[22] N.B. Karayiannis, P.-I. Pai, IEEE Trans. Image Process. 4 (1995) 1193.
[23] H.B. Kekre, T.K. Sarode, Int. J. Comput. Sci. Inf. Technol. (IJCSIT) 1 (2009) 7.
[24] J.Z. Sun, V. Misra, V.K. Goyal, IEEE Trans. Signal Process. 61 (2013) 3495.
[25] X.-l. Tu, M. Huang, Q.-b. Lu, J.-w. Wang, L.-l. Pei, Spectro. Spectr. Anal. 33 (2013) 1401.
[26] A. Zabala, X. Pons, Int. J. Remote Sens. 34 (2013) 2796.
[27] X. Tang, W.A. Pearlman, Three-dimensional Wavelet-based Compression of Hyperspectral Images, Springer US2006, pp. 273–308.
[28] A.J.S. Dutra, W.A. Pearlman, E.A.B.d. Silva, Compression of hyperspectral images with LVQ-SPECK, in: Data Compression Conference, 2008. DCC 2008, Snowbird, UT, 2008, pp. 93–102.
[29] J. Zabalza, J. Ren, J. Ren, Z. Liu, S. Marshall, Structured covariance PCA for real-time onsite feature extraction and dimensionality reduction in hyperspectral imaging, Appl. Opt. 53 (20) (2014) 4440.
[30] J. Ren, J. Zabalza, S. Marshall, J. Zheng, Effective feature extraction and data reduction with hyperspectral imaging in remote sensing, IEEE Signal Proc. Mag. 31 (July(4)) (2014) 149.
[31] J. Zabalza, J. Ren, M. Yang, Y. Zhang, J. Wang, S. Marshall, J. Han, Novel folded-PCA for improved feature extraction and data reduction with hyperspectral imaging and SAR in remote sensing, ISPRS J. Photogramm. Remote. Sens. 93 (7) (2014) 112.

[32] J. Zabalza, J. Ren, Z. Wang, S. Marshall, J. Wang, Singular spectrum analysis for effective feature extraction in hyperspectral imaging, IEEE Geosci. Remote. Sens. Lett. 11 (11) (2014) 1886.

[33] C. Zhao, X. Li, J. Ren, S. Marshall, Improved sparse representation using adaptive spatial support for effective target detection in hyperspectral imagery, Int. J. Remote Sens. 34 (24) (2013) 8669.

[34] J.C. Dunn, A fuzzy relative of the ISODATA process and its use in detecting compact well-separated clusters, J. Cybern. 3 (32) (1973) 1973.